Time-Spectral Method for CFD Prediction of Helicopter Rotor Vibratory Loads

Seongim Choi[1] and Anubhav Datta[2]

[1] Dept. of Aeronautics and Astronautics, Stanford University, Stanford, CA, 94305 sichoi@stanford.edu
[2] Eloret Corporation, NASA Ames Research Center, Moffett field, CA, 94035 adatta@mail.arc.nasa.gov

Summary. A Fourier collocation based time-spectral method is used to simulate helicopter rotor flows under high-speed transonic and highly-loaded dynamic stall conditions. Computations are performed using fully coupled CFD/Comprehensive Analysis, where the Comprehensive Analysis supplies finite element CSD and aircraft trim capabilities. The focus is on the prediction of vibratory airloads of an isolated rotor. The accuracy of spectral method is compared with a time-accurate analysis, both trimmed consistently to the same flight condition. Two UH-60A flights are simulated – Counters 8534 and 9017 from the U. S. Army/NASA Airloads Program – a high vibration flight and a deep dynamic stall flight. For the high vibration flight, the fastest and minimal implementation of the method, with 11 time instances for a 4-bladed rotor, predicts the vibratory lift and pitching moments within 5–10% accuracy of time-accurate simulations in about one-fifth the computational time. The largest errors occur in vibratory chord forces (10 to 20%). The minimal implementation is not adequate under dynamic stall conditions, as expected, where significant higher-harmonic content (6/rev and higher) produce aliasing errors in the harmonics of interest.

1 INTRODUCTION

The objective of this study is to demonstrate the potential of time-spectral CFD for simulating realistic rotorcraft flows using CFD/Comprehensive Analysis (CFD/CA) coupling. The highest levels of vibratory loads for a helicopter rotor occur in steady level flight characterized by periodic dynamics of the rotor blades. The motivation behind the time-spectral method is the fast and efficient extraction of a limited set of desired airload harmonics depending on the flight conditions and the objective of the design study – performance, loads, or vibration. In addition, its pseudo steady-state formulation opens opportunity for applying adjoint-based design optimization methods to the unsteady rotor problem. The focus of this preliminary investigation is on airloads prediction.

The spectral method implemented in this paper, is a standard algorithm based on the Fourier collocation method [1], where the periodic solution at each Fourier node is approximated by a discrete Fourier expansion. The idea of the time-spectral method is to apply the Fourier spectral method to the temporal discretization rather than to the conventional spatial discretization. A number of engineering problems which involve unsteady periodic motions have recently used time-spectral methods, such as turbomachinery [2] and flapping wing analysis [3]. An initial implementation of time-spectral method to simulate helicopter rotor flows was conducted in our previous studies for uncoupled, aerodynamics only, simulations for the UH-60A Black Hawk helicopter at several important level flight conditions [4, 5]. A first principles loads prediction require – CFD, CSD, and a solution procedure for simultaneously determining the rotor operating state. The operating state is determined by the vehicle flight dynamics (VFD) – trajectory and control pitch angles. In steady flight, VFD is simple: the trajectory is trivial, and the control angles are determined by the coupled trim procedure. The purpose of the present paper is to carry out fully coupled CFD/CA simulations.

The procedure for coupled CFD/CA in steady flight was originally proposed by Tung et al. in 1986 [6]. It is widely applied today and is well-known as *delta* or *loose* coupling procedure. There are no procedures, yet, for unsteady maneuvers. The *delta* or *loose* coupling procedure is implied in rotorcraft literature by the frequent use of the term CFD/Comprehensive Analysis. Though used interchangeably with CFD/CSD, it implies an analysis which uses both the CSD and trim models of current comprehensive codes, while replacing its lower order lifting-line (or surface) aerodynamic model with CFD. The solution procedure is iterative, and ensures strict time accuracy of response harmonics via trim iterations. It is therefore not the same as loose coupling as referred to in fixed-wing CFD/CSD. A review of the current state-of-the-art in helicopter rotor loads prediction using CFD/CA coupling can be found in ref. [7]. All of the current CFD methods have used a time-marching or time-accurate procedure.

The efficiency of TS method can make the coupling procedure less time consuming than a conventional time accurate computation – depending on the number of time instances chosen. In this paper 11 times instances are chosen, with a Nyquist frequency of 5/rev – a minimal requirement for predicting the dominant vibratory harmonics (3,4, and 5/rev) of a 4-bladed rotor. Two flight conditions of the UH-60A helicopter are chosen for validation. These are the flight Counters 8534 and 9017 of the U. S. Army/NASA UH-60A Airloads Program – the details of which are given in the results section.

The paper is organized into four sections. Following this introduction, the theoretical background and the mathematical formulation of the time-spectral method are described in Section 2. The details of the Comprehensive Analysis and CFD/CA coupling method are summarized in Section 3. The coupled CFD/CA predictions are described in Section 4.

2 TIME-SPECTRAL METHOD

2.1 Mathematical Formulation

The Navier-Stokes equations in a semi-discrete form can be written as

$$V\frac{\partial u}{\partial t} + R(u) = 0, \quad u = \begin{pmatrix} \rho \\ \rho u' \\ \rho v' \\ \rho w' \\ \rho E \end{pmatrix}, \tag{1}$$

where u is the vector of conservative variables, and $R(u)$ is the residual of spatial discretization of viscous, inviscid, and numerical dissipation fluxes. If we approximate u by a discrete Fourier series at N integer points,

$$u_j^N = \sum_{k=-N/2}^{N/2-1} \tilde{u}_k e^{ikt_j} \quad (j = 0, ..., N-1), \quad \text{where} \quad t_j = \frac{T}{N} j \ , \tag{2}$$

and T is a period, and u_j^N represents the truncated Fourier series of u up to N. A $\tilde{u}_k$ is a discrete Fourier coefficient of the variable u defined as follows,

$$\tilde{u}_k = \frac{1}{N} \sum_{j=0}^{N-1} u_j^N e^{-ikt_j} \quad k = -N/2, ..., N/2-1 \tag{3}$$

For the collocation method Equation 1 is required to be satisfied at each point,

$$\frac{\partial u_j^N}{\partial t} + R(u_j^N)|_{t=t_j}, \quad j = 0, 1, ..., N-1 \tag{4}$$

On the other hand, a differentiation of u in physical space can be obtained by the inverse transformation of the discrete Fourier coefficients multiplied by ik. Then the approximate derivative at the grid points are given by

$$(\mathcal{D}_N u)_l = \sum_{k=-N/2}^{N/2-1} a_k e^{ikt_l} \quad (l = 0, 1, ..., N-1), \ \text{where} \ a_k = ik\tilde{u_k} = \frac{ik}{N} \sum_{j=0}^{N-1} u_j^N e^{-ikt_j} \tag{5}$$

Equation 5 can be reprented by a matrix form by combining two terms in Equation 5,

$$(\mathcal{D}_N u)_l = \sum_{j=0}^{N-1} (D_N)_{lj} u_j^N, \quad \text{where} \ (D_N)_{lj} = \frac{1}{N} \sum_{k=-N/2}^{N/2-1} ike^{ik(t_l - t_j)} \tag{6}$$

Application of Fourier collocation derivative type operator to Equation 4 renders it as below,

$$D_N U + R(U) = 0, \quad \text{where } U \text{ is a vector form of } (u_0^N,\ u_1^N, ..., u_{N-1}^N) \tag{7}$$

If a pseudo-time derivative term is directly added for a time integration, then Equation 6 can be represented as below,

$$V\frac{\partial u_j^N}{\partial \tau} + V D_N u_j^N + R(u_j^N) = 0 \ (j = 0, 1, 2, ..., N-1) \ . \tag{8}$$

and Equation 8 is the final form of the equation we are employing. Compared to the original Equation 1, Equation 8 has a simpler form as a steady-state formulation. A matrix form of derivative operator can be written as a closed form as below with a odd number of grid points (time instances),

$$(D_N)_{lj} = \begin{cases} \frac{1}{2}(-1)^{l+j} cosec(\frac{(l-j)\pi}{N}) & : l \neq 0 \\ 0 & : l = j \ . \end{cases} \tag{9}$$

This matrix is skew-symmetric and the corresponding eigenvalues are $ik,\ k = -(N-1)/2, .., (N-1)/2$, with a odd number N. If we have a odd number of time instances, then eigenvalue of zero has single multiplicity rather than double multiplicity in the case of even number of time instances. For this reason, we choose to have a odd number of time instances for spectral formulation in our study for a stability issue related to the eigenvalues [8].

2.2 Convergence, Accuracy and Efficiency of Time-Spectral Method

The spectral accuracy is major attractiveness of the Fourier spectral method. Its convergence rate is ideally faster than any negative power of N, if u is N-times continuously differentiable and their derivatives up to $N-2$ are periodic [8]. If the band-width of the underlying waveforms is known and the number of sampling points are more than Nyquist rate, then spectral accuracy can be achieved.

However, the real waveforms we encounter in rotor flow analysis, such as the sectional airloads, are highly nonlinear and not band-limited, smoothness of their variation in time is not guaranteed, and the availability of the differentiation is not known a priori. Therefore the time-spectral method for the rotor flow analysis is inevitably under the influence of errors which are common to a classical Fourier collocation method, i.e. truncation error and aliasing error.

The issues to be addressed are: With respect to a varying number of time instances, 1) how is the convergence of the solutions? 2) how accurate are the solutions? 3) how much of computational time savings can we have to preserve a certain level of accuracy?

A study on those issues was carried out in our previous work [9] by directly comparing the time-accurate solutions and the time-spectral results with different number of time instances. Details are referred to Reference [9], and only a brief summary is given here. A high speed flight of UH-60A was simulated

by both computational methods. A different number of time instances varying from 3, 5, 9, 13, 17, to 23 were used for time-spectral computation. Aliased time-accurate solutions through an inverse FFT using a number of harmonics less than the Nyquist frequency of the original waveform were constructed and compared with the time-spectral solutions with the same number of harmonics. Percentile L^2 norms between two solutions were calculated with respect to the number of time instances, and several significant facts were realized. The key conclusions we can make on the convergence and accuracy of the time-spectral method were that: 1) the aliasing error decreases as we increase the number of time instances. 2) convergence rate is nearly exponential as the number of time instances increases. 3) With the number of time instances as small as around 20, we can achieve the accuracy within $1 \sim 2\%$ errors. Also this number of time instances can resolve the phenomena dominated by the critical vibratory frequencies (3,4,5 /rev and 7,8,9 /rev).

However, it should be noted that this conclusion can not be generalized for all rotor flow analysis and depend on the characteristics of the airloads waveform. Therefore if the airloads do not show smooth variation during a period, then the effects of the aliasing errors may not be negligible even with reasonably large number of time instances.

The effect of the number of time instances on the efficiency of the time-spectral method is also discussed several times in our previous work [4, 9]. A direct comparison of total wall-clock CPU time was made between time-accurate and time-spectral computation. As the number of time instance increases, the time increment is not linear and its slope is gradually increasing. A computation time for a multigrid cycle is the addition of time for space discretization and for spectral derivative term (see Equation 8), and is typically dominated by the space discretization which have operating counter of $O(N)$ for the finite-difference method. Thus, at a small number of time instances, computation time for the spectral derivative term is negligible and increase in time is dominated mostly by linear contribution from space discretization. However, as the number of time instances becomes large, computation time for the derivative term with operating counter of $O(N^2)$ (of multiplication of matrix and vector) can not be neglected and the quadratic increase is gradually reflected in total time.

A direct comparison of total wall-clock CPU time to obtain the converged solutions is made between time-accurate and time-spectral computation to see the efficiency of the time-spectral method. A rigorous comparison between the two methods, thus, requires a certain degree of flexibility considering the characteristics of the problems we solve and the level of convergence we want to achieve. Nevertheless time-spectral computation has shown more than the factor of at lease two or three for all simulations in our previous [4, 5] and the current simulation using up to as many as 25 time instances.

2.3 Implementation: SUmb solver

Three-dimensional compressible Navier-Stokes flow solver, SUmb (Stanford University multi-block), has been utilized for all computations in this paper. SUmb is a multi-block structured flow solver developed at Stanford University under the sponsorship of the Department of Energy Advanced Strategic Computing (ASC) program. Various turbulence models are implemented to capture the viscous and turbulent properties of the flow: Baldwin-Lomax, Spalart-Allmaras, $k-\omega$, Menter SST, v^2-f. SUmb is a massively parallel code (in both CPU and memory) using scalable pre-processor, load balancing, and MPI. It employs multigrid, Runge-Kutta time stepping for the mean flow, and DD-ADI solution methodology for the turbulence equations. Central difference discretization (second order in space) with several artificial dissipation options (scalar or matrix), or upwind discretization is available for a space discretization. For unsteady time integration, second-/third-order backwards difference formula(BDF [10]) or the time-spectral approach for time-periodic flows can be used. SUmb has been successfully used in many applications including simulation of launch vehicles, space and re-entry vehicles, jet/turbo engines, subsonic and supersonic aircraft, and helicopters. A second order BDF scheme was used for the time-accurate computation, and a second order upwind scheme with Roe's flux differencing for the inviscid fluxes. Spalart-Allmaras turbulence model was used for the computation of the viscous flux and the turbulence.

3 CFD / Comprehensive Analysis Coupling

The Time-spectral analysis is coupled to the rotorcraft comprehensive analysis UMARC (University of Maryland Advanced Rotorcraft Code) [11]. The comprehensive code can carry out trim, flutter, and ground and air-resonance solution procedures using its internal unsteady lifting-line based aerodynamic model. The purpose of CFD coupling is to replace the simple aerodynamic model with CFD, within the trim solution procedure, for the prediction of airloads and structural loads.

3.1 UMARC Comprehensive Analysis

During the coupled solution procedure, UMARC provides the CSD and trim capabilities, and in addition, the aerodynamic sensitivities to blade deformations as required by the delta method. The details of the modeling, methodologies, and validation can be found in Ref. [12]. The UH-60A rotor model, and the analysis is identical to the one used for the original CFD/Comprehensive Analysis coupling studies with the overset TURNS code [7].

Two different trim procedures are used in this study: an isolated rotor trim, and a full aircraft trim. In an isolated trim, the three rotor control

angles (collective, longitudinal and lateral cyclic angles) are determined using a target thrust and the two hub moments, pitch and roll. The shaft tilt angles with respect to on-coming flow are prescribed. In a full aircraft trim, the three rotor control angles, the two aircraft longitudinal and lateral tilts, and the tail rotor collective are calculated based on three forces and moments equilibrium about the aircraft center of gravity. The fuselage aerodynamic properties including the horizontal tail and tail rotor properties, that are necessary for this procedure, are included via look up tables and lower order aerodynamic models within the comprehensive analysis [11].

3.2 Coupled Solution Procedure

The delta coupling procedure is a domain partitioned procedure. Airloads from the CFD domain and blade deformations from the CSD domain are exchanged over one period of a steady-state solution. In the present study, the CSD time discretization is an integer multiple of the CFD time discretization. Thus, the airloads are available directly at the CSD time steps. The deflections are interpolated linearly at the CFD time steps. The coupled solution procedure is as follows.

1. Obtain a lifting-line comprehensive analysis solution. This provides the baseline blade deformations, trim angles, and airloads.
2. Calculate CFD airloads using the baseline blade deformations and trim angles. The CFD airloads are, in general, different and improved from the baseline airloads.
3. The difference between the CFD airloads obtained in step 2 and lifting-line airloads are the delta airloads. The lifting-line comprehensive analysis is now re-performed, but with the delta airloads imposed in addition to the intrinsic lifting-line airloads. The delta airloads are held fixed over the comprehensive analysis trim iterations. The lifting-line airloads change from one trim iteration to another and provide the airload sensitivities that are required to trim the rotor. In addition, the lifting-line airloads provide aerodynamic damping which makes the procedure well-posed and stable.
4. Step 2 and Step 3 is one CFD/CSD iteration. The iterations are performed until the delta airloads converge at every radial and azimuthal station.

A simple lifting-line model suffices, as long as it provides the airload sensitivity to blade deformations correctly. Here, a linear inflow, and a linear aerodynamic model is used. Approximately 6 to 8 iterations is necessary for a converged solution. The converged airloads are entirely CFD airloads.

The fluid-structure interface is simple. The CFD airloads are linearly interpolated from the CFD grids to all CSD Gauss points – a total of 120 Gauss points from root to tip – as sectional normal force, chord force, and pitching moment (at 1/4-chord) distributions. These are obtained by the integration of CFD pressures and surface shears along chord-wise strips, a natural choice

for structured grids. The CSD deformations are linearly interpolated from the CSD Gauss points to all CFD span-wise grid stations – a total of 65 span-wise stations from root to tip.

4 Results

The flight C8534 is one of the highest vibration flights for this helicopter, with high levels of vibratory airloads at 3,4, and 5/rev. The flight C9017 is a deep dynamic stall flight occuring at the very limit of the level-flight thrust boundary. The high frequency pitching moments, 4/rev and higher, and the consequent pitch link loads have a pattern similar to severe maneuvers – loads that determine the design loads for the pitch link and swash plate components in the fixed frame.

The contributions of CFD (as compared to conventional lifting-line models) in resolving the key aeroelastic mechanisms have been the most significant in these two flights. The key mechanisms have recently been well understood, and CFD/CA coupled predictions well benchmarked for both these flights [7]. Therefore, these two flights are chosen for validation.

The time-spectral predictions for the two flights are described below. For each flight, a short description of the key aeroelastic mechanisms is provided in the beginning.

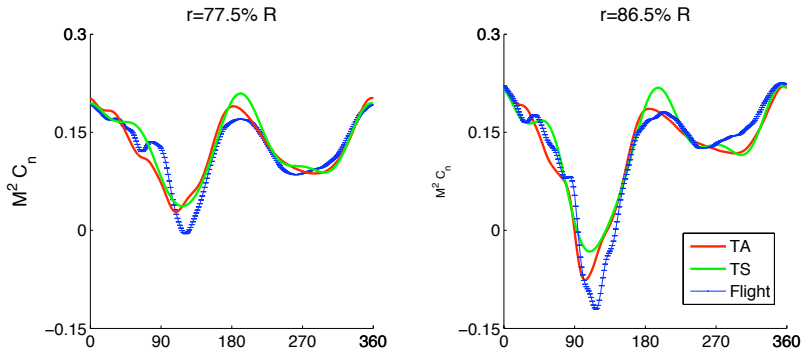

Fig. 1. Measured and predicted normal forces for the UH-60A in high speed flight C8534; red-TA; green-TS; symbols-Flight

4.1 High speed flight C8534

This flight has a speed ratio $\mu = 0.368$ (155 kts), vehicle weight coefficient to solidity ratio $C_W/\sigma = 0.0783$, and a longitudinal shaft tilt angle of α = -7.31° (tilt-forward). The predicted thrust level (along shaft) is $C_T/\sigma =$

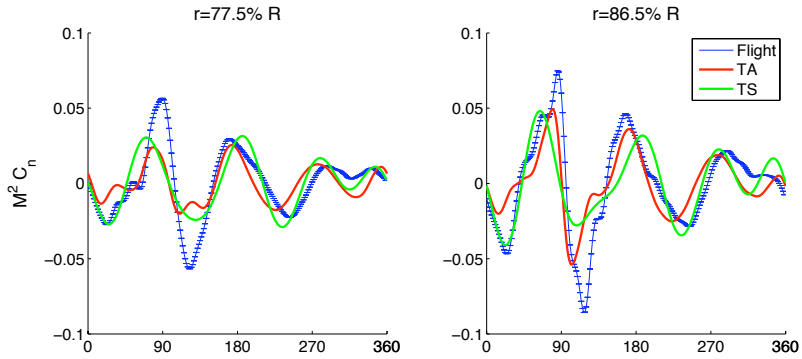

Fig. 2. Measured and predicted vibratory normal forces (3/rev and above) for the UH-60A in high speed flight C8534; red-TA; green-TS; symbols-Flight

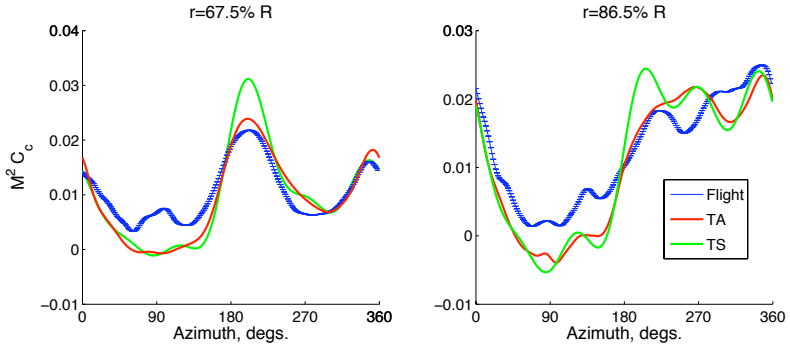

(a) Chord forces: + ve towards leading edge

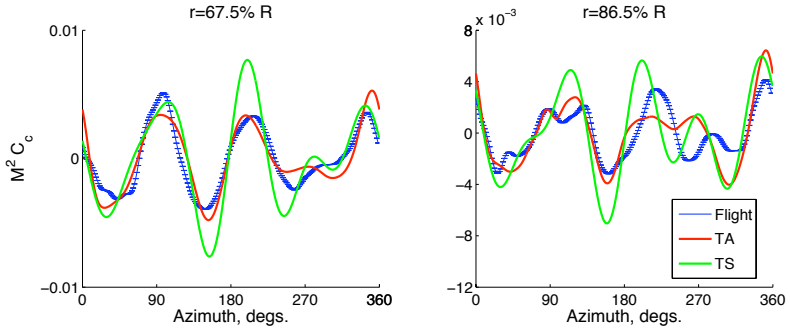

(b) Vibratory chord forces: 3/rev and above

Fig. 3. Measured and predicted chord forces for the UH-60A in high speed flight C8534; red-TA; green-TS; symbols-Flight

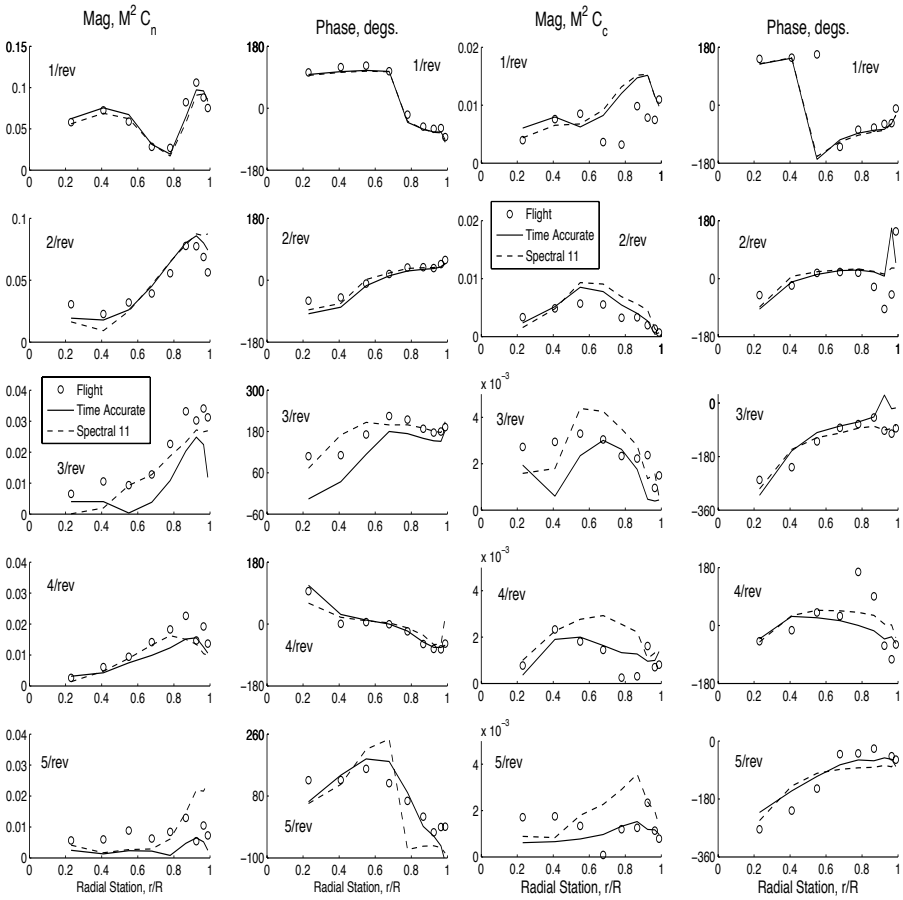

Fig. 4. Normal force harmonics (1–5/rev) in magnitude and phase varying over blade span; high speed flight C8534

Fig. 5. Chord force harmonics (1–5/rev) in magnitude and phase varying over blade span; high speed flight C8534

0.084, around 17,500 lb. The rotor roll and pitch moments, measured from shaft bending gages, are around 6000 ft-lb (roll left) and 4200 ft-lb (pitch up) respectively. The trim analysis targets the thrust and two hub moments at the prescribed shaft tilt angle to solve for the three rotor control angles.

The primary mechanism of vibratory airloads in this flight is the large elastic twist deformation of the blade in response to three-dimensional, unsteady, transonic pitching moments near the tip on the advancing side. The secondary mechanism, occurring in presence of the correct twist, is an inboard wake interaction on the advancing side. In the case of rotors with negative lift near the tip, like the UH-60A, the trailed vorticity moves inboard in the azimuths of negative lift and creates a secondary lift impulse on the follow-

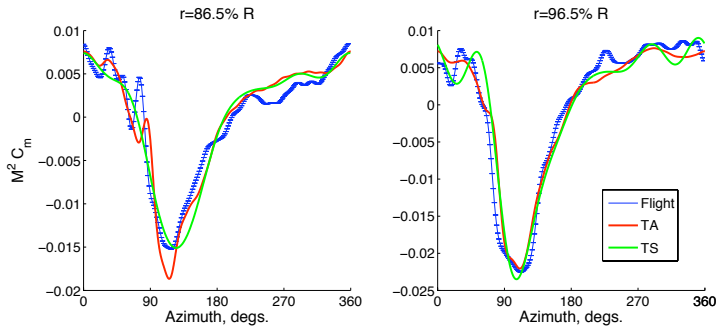

Fig. 6. Measured and predicted quarter-chord pitching moments for the UH-60A in high speed flight C8534; mean removed; red-TA; green-TS; symbols-Flight

ing blade at the junction of the first and second quadrant. This impulse is a significant source of vibratory harmonics.

The predicted normal forces at two blade sections are shown in Fig. 1. Note that both the time-accurate and time-spectral results are fully coupled first principle solutions. The trim conditions are identical but the blade deformations are different. The time-accurate results are similar to benchmarked results [7] at all radial stations. As per the study reported in Ref. [9] about 10% spectral error is expected in normal forces from aliasing at this flight with 11 time instances. The impact of these errors on the vibratory harmonics is shown in Fig. 2. Note that for 11 time instances the Nyquist frequency is $(11-1)/2 = 5$/rev. Thus a 6/rev content in the underlying waveform (time-accurate) will fold on to 5/rev, 7/rev to 4/rev, 8/rev to 3/rev and so on. Thus the vibratory harmonics 3,4, and 5/rev are influenced by 8,7, and 6/rev respectively. The predicted chord forces are shown in Fig. 3. The time-accurate prediction in chord loads is unsatisfactory in itself, but that study is beyond the scope of the present paper. Here, we focus on the comparison between time-accurate and time-spectral results.

The radial distribution of the harmonics are shown in detail in Figs. 4 and 5. The 1/rev normal force phase shows that the trim conditions are identical between the two simulations. As 1 and 2/rev (and the steady) are in general in good agreement, 11 time instances appear to be adequate for performance calculations – at least for this flight condition, as there is no significant aliasing from 11, 10, and 9/rev. The largest error in vibratory harmonics occurs in 5/rev. The errors in 3 and 4/rev are relatively lower. This will result in a somewhat acceptable structural load as the first flap bending frequency lies between 3 and 4/rev (3.28/rev). For the chord forces, the aliasing errors follow the same trend as normal forces – largest in 5/rev (more than 100%) followed by 4 and 5/rev. Compared to normal force, the penalty paid due to aliasing errors in chord-forces will be more severe on the lead-lag dynamics as the first

chord bending frequency sits between 4 and 5/rev for this rotor (4.66/rev). We note, however, that the errors always over-predict by definition and thus always provides conservative loads estimates for design.

The predicted pitching moments are shown in Figs. 6. The pitching moments drive the key vibratory loads mechanism (large elastic twist deformation) in this flight. The three-dimensional, unsteady, transonic tip relief effect that generates the impulsive wave form in the first quadrant is well predicted by both time-accurate and time-spectral method. The effect of this mechanism is mainly on the 1 and 2/rev pitching moments and therefore, as expected, there is little aliasing error in the waveform. The spectrum of the time-accurate pitching moment waveform is more band-limited compared to the sectional forces and hence there is little error even in the vibratory harmonics.

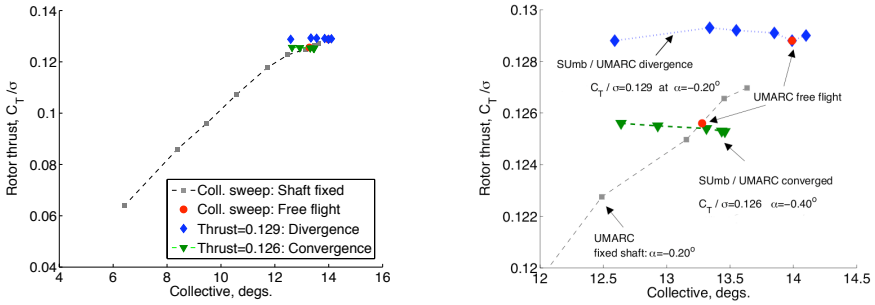

(a) Collective sweep from 6° to 14°

(b) Stall region magnified

Fig. 7. Collective sweep of the UH-60A rotor at $\mu = 0.237$; determination of the maximum thrust capability of the CFD/CA analysis at and near stall flight C9017

4.2 Dynamic Stall Flight C9017

This flight has $\mu = 0.237$, $C_W/\sigma = 0.1325$, and α = -0.19° (tilt-forward). The predicted thrust level (along shaft) is $C_T/\sigma = 0.129$, around 16,500 lb. The rotor roll and pitch moments are very low, around 320 ft-lb (roll left) and 112 ft-lb (pitch up) respectively.

As the flight lies close to the stall boundary, the approximate analysis stall boundary is first determined, see Fig. 7. Targeting the above hub moments and shaft angle, a thrust sweep is performed with baseline UMARC. The baseline UMARC uses an unsteady lifting-line model that combines free wake, a Weissinger-L near wake, 2D airfoil tables, and Leishman-Beddoes semi-empirical dynamic stall [12]. The rotor thrust levels off at a maximum of C_T/σ= 0.1265. With a shaft free full aircraft trim, with the measured weight coefficient C_W/σ=0.1325, a maximum thrust of C_T/σ= 0.129 is attained. The UMARC/overset TURNS coupled solution in Ref. [7] was trimmed at

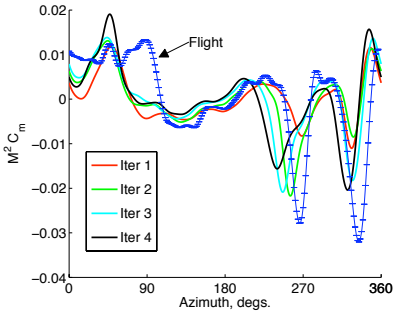

(a) Diverged pitching moment predictions for $C_T/\sigma = 0.129$; flight C9017

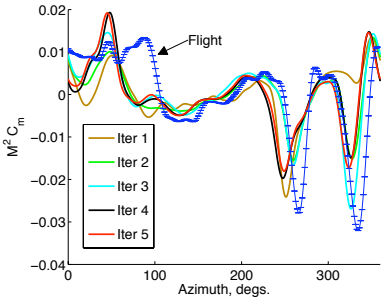

(b) Converged pitching moment predictions for $C_T/\sigma = 0.126$; reduced thrust C9017

Fig. 8. Evolution of predicted quarter-chord pitching moments (at 86.5% R) for stall flight C9017, and a 2.5% reduced thrust flight near C9017, using time-accurate CFD

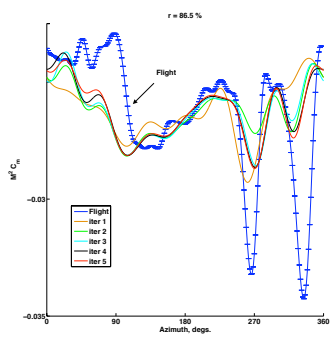

(a) r/R = 86.5 %

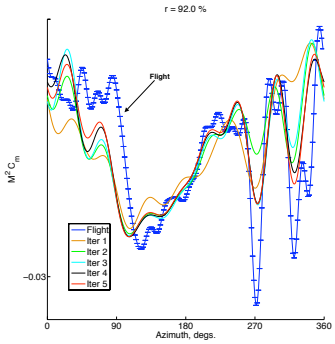

(b) r/R = 92.5 %

Fig. 9. Evolution of predicted quarter-chord pitching moments for the reduced thrust flight near C9017 using time-spectral CFD

this condition. The present UMARC/SUmb solution failed to converge at this condition. As shown by the blue symbols in Fig. 7, the collective requirement increases continuously with each CFD iteration. Note that this is similar to the CAMRAD-II/OVERFLOW-2 studies. Earlier, OVERFLOW-D had obtained a trim solution at C_T/σ=0.129 [7] which could not be re-produced subsequently with a corrected turbulence model in OVERFLOW-2. To avoid spurious results the aircraft weight coefficient is is therefore reduced by 2.5% in the present study. A free flight trim is now carried out with a weight coefficient of C_W/σ=0.1285. This leads to a trim thrust level of C_T/σ=0.126 at a shaft angle of -0.40°.

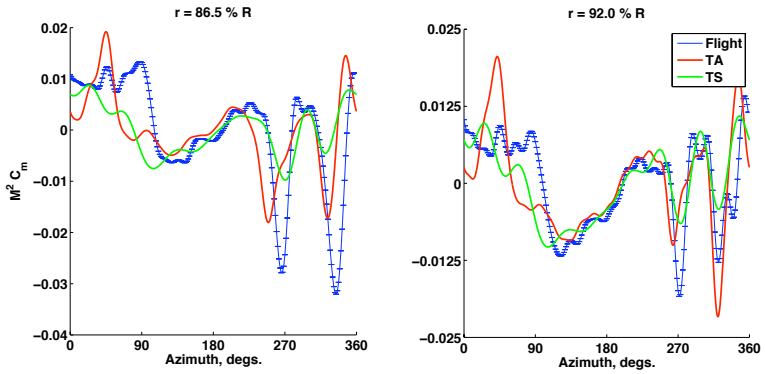

Fig. 10. Measured and predicted quarter-chord pitching moments for the reduced thrust flight near C9017; red-TA, green-TS, symbols-Flight

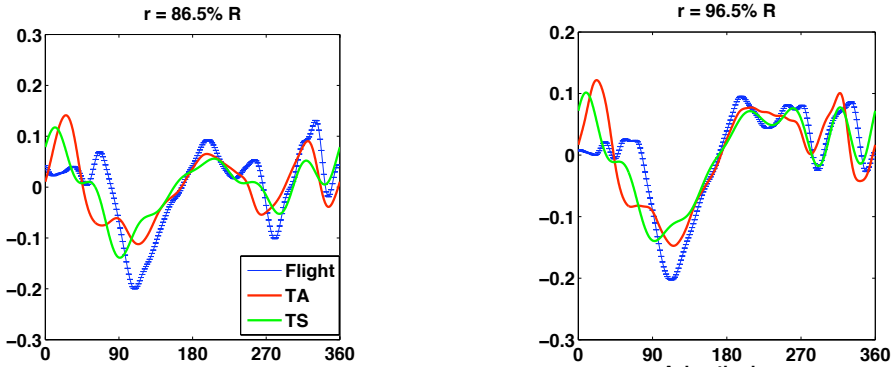

Fig. 11. Measured and predicted normal forces for the reduced thrust flight near C9017; red-TA, green-TS, symbols-Flight

The evolution of the predicted pitching moments with coupling iterations, for both the divergent and convergent trim conditions, are shown in Fig. 8 using time-accurate CFD. The shifting stall pattern of the gradually diverging solution is consistent with the physics of the two stall cycles. The two cycles are related to the sectional trim angles and elastic twist deformations [7]. The first cycle is a trim stall – triggered by the rise in the sectional angle of attack due to high cyclic pitch angles. Note that the pitch angles in this flight are lower compared to high speed, but the shaft angle is nearly zero – only 0.19° compared to 7.31° in high speed. The second cycle was related to an elastic twist peak occurring in the fourth quadrant – generated by 4 and 5/rev torsion. The cycle triggers the 4 and 5/rev elastic twist response producing the second stall. The first torsion frequency of the rotor lies between

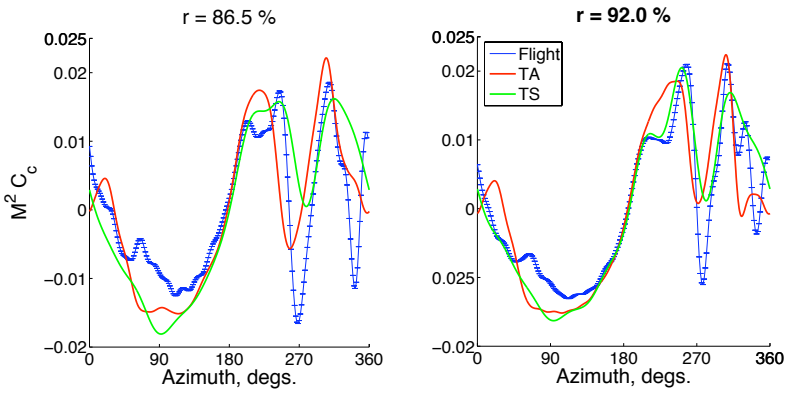

Fig. 12. Measured and predicted normal forces for the reduced thrust flight near C9017; red-TA, green-TS, symbols-Flight

4 and 5/rev (4.38/rev). During divergence, as shown in Fig. 8, the trim stall occurs progressively earlier in azimuth as more and more pitch angles are required for trim. In contrast, during convergence the stall pattern gradually settles at a given azimuth location. The convergence pattern for the time-spectral predictions are of course to time-accurate, Fig. 9. The time-spectral and time-accurate predictions are compared in Fig. 10. As expected, with only 11 time-instances there is a significant under-prediction of the two stall peaks. In addition significant errors accumulate from aliasing, particularly due to a high 6/rev content in this flight which folds on to 5/rev. However, as shown in Ref. [9], this error can be quantified once a time-accurate solution is obtained, and a suitable number of time instances decided upon for subsequent design runs. Note that, a total of 17 time-instances was recommended in Ref. [9] for this rotor.

The oscillatory (mean removed) normal and chord forces are shown in Figs. 11 and 12. Compared to the high speed case, the time-accurate predictions show significant discrepancies with test data. The retreating blade pre-stall trough, in the third quadrant, is a recognized discrepancy of the current state-of-the-art. The advancing blade waveform is influenced more by the wake, and the present coarse grid resolution (around 4M grid points), used for the stall flight, appears inadequate for a multi-block type grid.

5 CONCLUSIONS AND FUTURE WORK

A Fourier collocation based time-spectral CFD was implemented to simulate realistic rotor flows using fully coupled CFD/Comprehensive Analysis procedure. The predicted vibratory airloads were compared with time-accurate simulations, consistently, at the same flight conditions, as well as with flight

test data of the UH-60A helicopter. Two important level flight conditions were simulated - a high speed, high vibration flight, and a moderate speed, highly-loaded, dynamic stall flight. The stall flight was trimmed to a 2.5% reduced thrust level based on a collective sweep study.

The spectral simulations were performed using only 11 time instances – the minimal requirement for predicting the dominant vibratory harmonics of a four-bladed rotor. Compared to time-accurate simulations, the spectral error in the high vibration flight, is less than 5% in pitching moments, approximately 5–10% in vibratory normal force, and 10–20% in vibratory chord force. The computational time is approximately 1/5. As expected, 11 time instances were not adequate for the stall flight. The 6/rev and higher harmonics folded on to the lower frequencies producing significant amounts of aliasing errors. It is concluded, based on this study, that the time-spectral method can be used effectively for the prediction of rotor vibratory loads, with a suitable choice of time instances. The method can be particularly attractive if equipped with anti-aliasing filters.

The method is attractive as it opens opportunity for adjoint-based optimization of the unsteady problem. An isolated, aerodynamics only optimization have limited value in rotary wing dynamics – the present method has the potential for a coupled CFD/CA optimization procedure.

References

1. Canuto, C., Hussaini, M. Y., Quarteroni, A., and Jr. Zang, T. A., T. A., Jr. Zang "Spectral Methods in Fluid Dynamics," *Springer,* 1998.
2. Van der Weide, E., Gopinath, A., and Jameson, A., "Turbomachinery applications with the time spectral method," *AIAA Paper 05-4905*, Toronto, Canada, Jun. 2005.
3. Sankaran, S., Gopinath, A., Van der Wedie, E., Kim, S., Tomlin, C., and Jameson, A., "Aerodynamics and Flight Control of Flapping Wing Flight Vehicles: A Preliminary Computational Study," *AIAA Paper 05-0841*, Reno, NV, Jan. 2005.
4. Choi, S., Alonso, J. J., Van der Weide, E., and Sitaraman, J., "Validation Study of Aerodynamic Analysis Tools for Design Optimization of Helicopter Rotors," *AIAA Paper 07-3929*, Miami FL., June 2007.
5. Choi, S., Lee, K. H., Alonso, J. J., and Datta, A., "Preliminary Study on Time-Spectral and Adjoint-Based Design Optimization of Helicopter Rotors," *AHS specialist meeting*, San Francisco, CA., Jan 2008.
6. Tung, C., Cardonna, F.X., and Johnson, W.R., "The Prediction of Transonic Flows on an Advancing Rotor," *Journal of the American Helicopter Society*, Vol. 31, (3), July 1986, pp. 4–9.
7. Datta, A., Nixon, M. and Chopra, I., "Review of Rotor Loads Prediction with the Emergence of Rotorcraft CFD," *Journal of the American Helicopter Society*, Vol. 52, (4), October 2007, pp. 287–217.
8. Hesthaven, J., Gottlieb, S., and Gottlieb, D., "Spectral Methods for Time-Dependent Problems," *Cambridge Monographs on Applied and Computational Mathematics,* 2007.

9. Choi, S., and Datta, A., "CFD Prediction of Rotor Loads using Time-Spectral Method and Exact Fluid-Structure Interface" *26th AIAA Applied Aerodynamics conference, AIAA paper 08-7325*, Honolulu Hawaii, Aug. 2008.
10. Jameson, A., "Time dependent calculations using multigrid, with application to unsteady flows past airfoils and wings," *AIAA Journal, 91-1956,* June 1998.
11. Datta, A., Chopra, I., "Validation and Understanding of UH-60A Vibratory Loads in Steady Level Flight," *Journal of the American Helicopter Society*, Vol. 49, No. 3, July 2004, pp 271-287.
12. Datta, A., and Chopra, I, "Validation of Structural and Aerodynamic Modeling using UH-60A Airloads Program Data," *Journal of the American Helicopter Society*, Vol. 51, (1), January 2006, pp. 43–58.